



## Engineering surface Si-OH species for highly effective ethylene epoxidation on Ag/SiO<sub>2</sub> catalyst

Kaipeng Cao <sup>a,1</sup>, Min Huang <sup>a,1</sup>, Gang Wang <sup>a,b,c</sup>, Jie Li <sup>a,b</sup>, Chunshan Li <sup>a,b,\*</sup>

<sup>a</sup> State Key Laboratory of Mesoscience and Engineering, CAS Key Laboratory of Green Process and Engineering, Beijing Key Laboratory of Ionic Liquids Clean Process, Institute of Process Engineering, Chinese Academy of Sciences, Beijing 100190, PR China

<sup>b</sup> School of Chemical Engineering, University of Chinese Academy of Sciences, Beijing 101408, PR China

<sup>c</sup> Longzihu New Energy Laboratory, Zhengzhou Institute for Emerging Industrial Technology, Henan University, Zhengzhou 450000, PR China

### ARTICLE INFO

#### Keywords:

Ethylene epoxidation  
Support management  
Silver catalysts  
surface Si-OH  
EO selectivity

### ABSTRACT

The catalyst supports for ethylene epoxidation are conventionally limited to low-surface-area  $\alpha$ -Al<sub>2</sub>O<sub>3</sub> to suppress undesired secondary transformations of ethylene oxide (EO). In this work, high specific surface area SiO<sub>2</sub> was employed as a support. Systematic investigations reveal hydrogen-bonded silanol groups as a critical factor influencing EO selectivity through dual mechanisms. These groups significantly affect the desorption kinetics of surface species on Ag nanoparticles, potentially affecting the elementary steps of EO production. Furthermore, they also serve as active sites for EO secondary conversion. Thermal pretreatment (700 °C) for SiO<sub>2</sub> support effectively reduces hydrogen-bonded silanols via dehydration/condensation while retaining the silica's porous architecture. The resulting Ag/SiO<sub>2</sub> catalyst features ultrasmall Ag nanoparticles (~3 nm) and demonstrates exceptional performance of 81 % EO selectivity without requiring promoters. Furthermore, kinetic studies of the ethylene oxidation reaction were conducted to investigate the impact of silanol species on reaction. This study provides new insights into the influence of surface hydroxyls on ethylene epoxidation and offers a potential strategy for optimizing catalyst performance through controlled surface modification.

### 1. Introduction

Ethylene oxide (EO) is a highly significant raw material and synthetic intermediate, with extensive applications in the production of ethylene glycol, nonionic surfactants, alcohol ethers, and various other oxygen-containing downstream products. (Pu et al., 2019) The chlorohydrin process, initially employed for EO production in 1914, was progressively discontinued due to its hazardous nature and pollution issues. Currently, ethylene epoxidation stands as the synthetic principal route for large-scale EO production. In EO production processes, a major focus is placed on reducing the complete oxidation of both ethylene and EO (Chu et al., 2025; Soni et al., 2025). Therefore, precise control of the selective epoxidation reactions for EO synthesis is crucial, as improvements in catalyst selectivity can lead to significant capital savings and notable reductions in emissions. (Hus et al., 2023).

Despite the first report of the catalytic process for ethylene epoxidation in 1931 and ongoing research efforts, silver-based catalysts

remain the sole choice in the industrial sphere for this reaction. (Hwang et al., 2024) Research has shown that the delicate structure of the silver surface and reactive oxygen species, which can vary significantly across different facets, play a crucial role in determining both activity and selectivity. (Christopher and Linic, 2008; Hus and Hellman, 2019; Guo et al., 2024) The EO selectivity achieved by an unpromoted silver catalyst is around 50 %. (Christopher and Linic, 2008; van Santen and Kuijpers, 1987; Jalil et al., 2025) Numerous studies have been devoted to enhancing the performance of conventional Ag-based epoxidation catalysts through the use of promoters, such as Cs, Mo, Re, and SO<sub>4</sub><sup>2-</sup>, with the promoting mechanisms typically classified into geometric and electronic effects. (Hwang et al., 2024; Ramirez et al., 2016; Serafin et al., 1998; Diao et al., 2015; Keijzer et al., 2025; Keijzer et al., 2025; Salaev, 2021; Keivanimehr et al., 2025) Furthermore, Cl is incorporated into the catalytic system to facilitate the chlorine deposition on the catalyst surface, acting as a promoter. (Rocha et al., 2014; Pursell et al., 2003; Campbell and Paffett, 1984; Iyer and Bhan, 2024) Most recently,

\* Corresponding author at: State Key Laboratory of Mesoscience and Engineering, CAS Key Laboratory of Green Process and Engineering, Beijing Key Laboratory of Ionic Liquids Clean Process, Institute of Process Engineering, Chinese Academy of Sciences, Beijing 100190, PR China.

E-mail address: [csl@ipe.ac.cn](mailto:csl@ipe.ac.cn) (C. Li).

<sup>1</sup> These authors contributed equally to this work.

Jalil reported that the addition of Ni in a 1:200 Ni to Ag atomic ratio to supported Ag catalyst could provide a ~ 25 % selectivity increase. (Jalil et al., 2025) Additionally, the size of silver particles is acknowledged as another crucial factor influencing process selectivity. Silver particles sized from tens to hundreds of nanometers are typically required to achieve high EO selectivity (Sun et al., 2022; van den Reijen et al., 2017; Keijzer et al., 2024; Egelske et al., 2022; van Hoof et al., 2019). Under multiple optimization, a well-engineered catalyst can achieve an EO selectivity rate of 90 % with Cl co-flow. (Pu et al., 2019; Salaev et al., 2021).

The support also plays a crucial role in this reaction. Previous studies have underscored the challenge faced when employing high specific surface area oxides as supports for silver catalysts in ethylene epoxidation, as they often display inferior performance due to the surface's propensity for promoting the undesired decomposition of EO. (Yong et al., 1991; van den Reijen et al., 2019; Kanoh et al., 1979; Jain and Stangland, 2025) Triantafyllidis et al. (Fotopoulos and Triantafyllidis, 2007) compared the activity of silver catalysts supported on non porous  $\text{SiO}_2$ , silicates, aluminosilicates, and  $\alpha - \text{Al}_2\text{O}_3$  in ethylene epoxidation. They found that the selectivity of ethylene oxide on silver catalysts supported on mesoporous aluminosilicates was comparable to that of  $\text{Ag}/\alpha - \text{Al}_2\text{O}_3$  catalysts. However, mesoporous aluminosilicates have almost zero selectivity for ethylene oxide due to the presence of a small number of acidic sites on their surface. It is widely acknowledged that the secondary conversion of EO is strongly influenced by the acidic properties of the support. (Fotopoulos and Triantafyllidis, 2007; Lee et al., 1988; Bulushev et al., 1995) The EO precursors (intermediate species), initially formed on silver sites, undergo isomerization to acetaldehyde on either Lewis or Brønsted acid sites of the support. Acetaldehyde is subsequently oxidized on the silver sites, ultimately producing  $\text{CO}_2$ . Besides, hydroxyl groups have been reported to play a prominent role in the secondary conversion of EO. (van den Reijen et al., 2019) Nevertheless, the influence of support surface characteristics on the ethylene epoxidation reaction process and subsequent reactions remains poorly understood, hindering the development of high surface area supports for the process. (Mao and Vannice, 1995) Consequently,  $\alpha\text{-Al}_2\text{O}_3$  with low surface areas (<1  $\text{m}^2/\text{g}$ ) has predominantly been adopted to mitigate the conversion of EO.

In this study,  $\text{Ag/SiO}_2$  catalysts with ultrasmall silver nanoparticles (~3 nm) were prepared using high specific surface area  $\text{SiO}_2$  with varying surface properties for the ethylene epoxidation reaction. It's revealed that surface hydroxyls, particularly hydrogen-bonded silanol groups, play a primary factor contributing to the reduced selectivity of EO during the epoxidation reaction, and the mechanism was revealed. This work provides new insights into the effect of support on Ag catalyst, and offers a strategy for enhancing the product selectivity of the ethylene epoxidation reaction.

## 2. Experimental section

### 2.1. Materials and reagents

Silica ( $\text{SiO}_2$ , analytical grade, Shanghai Zhongye New Material Co., Ltd.); Silver nitrate ( $\text{AgNO}_3$ , analytical grade, Xilong Scientific Co., Ltd.);  $\text{N}_2$ ,  $\text{O}_2$ ,  $\text{C}_2\text{H}_4$ ,  $\text{H}_2$ ,  $\text{CO}_2$ , and EO standard gas (Containing 0.5 % ethylene oxide and balanced with 99.5 % nitrogen) are all supplied by Langfang Langwei Gas Co., Ltd.

### 2.2. Catalyst preparation

Amorphous silica ( $\text{SiO}_2$ ) was adopted as the support material for the preparation of  $\text{Ag/SiO}_2$  catalysts. The surface concentration of silanol ( $\text{Si-OH}$ ) groups on the  $\text{SiO}_2$  was regulated through heat treatment at temperatures of 500°C, 600°C, 700°C, and 800 °C respectively for a duration of 300 min each. Different batches of  $\text{SiO}_2$  were then subjected to equal volume impregnation with an aqueous silver nitrate solution to

achieve a typical silver loading of 15 wt% (the mass percentage of Ag relative to  $\text{SiO}_2$  is 15 %). Following the impregnation process, the samples were dried at 120 °C for an overnight period to obtain the  $\text{Ag/SiO}_2$  precursor. Afterwards, the samples were compressed and sieved into uniform granules (20–40 mesh) and subsequently activated *in situ* within the reaction tubes for the subsequent evaluation. This activation was conducted under a meticulously controlled atmosphere with a nitrogen to hydrogen ratio of 9:1, at a temperature of 350 °C, and was sustained for a period of 2 h. The reduced sample is referred to as  $\text{Ag/SiO}_2$  catalyst.

### 2.3. Characterization

X-ray diffraction (XRD) patterns were obtained on an X-ray diffractometer of PANalytical X'Pert PRO with  $\text{Cu K}\alpha$  radiation (scanning speed: 5°/min, scanning region: 10 ~ 90°). The morphologies of zeolites were acquired using Hitachi SU8020 scanning electron microscope (SEM). Transmission electron micrograph (TEM) images were obtained on a JEOL JEM-2100F microscope. Textural properties of the samples were obtained on a Micromeritics ASAP 2460 analyzer through  $\text{N}_2$  adsorption and desorption measurements. X-ray photoelectron spectroscopy (XPS) analysis was conducted on an ESCALAB 250Xi electron spectrometer.  $^1\text{H}$  NMR spectra were recorded on the AVANCE III HD 500 MHz resonant spectrometer from Bruker. Before test, samples were treated under vacuum at 350 °C for 6 h to remove the physically adsorbed water.

The oxygen temperature-programmed oxidation ( $\text{O}_2\text{-TPO}$ ) experiments were performed on a Micromeritics Autochem II 2920 equipped with a TCD detector. 0.1 g  $\text{Ag/SiO}_2$  catalyst was loaded into a U-shaped quartz tube and pretreated under flowing of a 10 %  $\text{H}_2$  in He gas mixture at a rate of 30 mL/min at 350 °C for 2 h. Subsequently, the sample was cooled to 50 °C, and the gas flow was switched to a 5 %  $\text{O}_2/\text{He}$  mixture (30 mL/min). The temperature was then linearly ramped from 50 °C to 350 °C at a rate of 10 °C/min. TCD signals were recorded to quantify oxygen consumption. Temperature programmed desorption of oxygen ( $\text{O}_2\text{-TPD}$ ) and ethylene ( $\text{C}_2\text{H}_4\text{-TPD}$ ) was performed on a Micromeritics Autochem II 2920 equipped with a mass spectrometer. All the experiment is conducted with 0.1 g sample, which was placed in a U-shaped quartz tube. Under a continuous flow of a 10 %  $\text{H}_2$  in He gas mixture at a rate of 30 mL/min, the sample was heated up to 350°C for a pretreatment period of 2 h. After the pretreatment process, the temperature was cooled down to 50°C, and a mixture of 10 %  $\text{O}_2$  (or  $\text{C}_2\text{H}_4$ ) in He was introduced with a flowing rate of 30 mL/min and maintained for 1 h to enable the samples to adsorb  $\text{O}_2$  (or  $\text{C}_2\text{H}_4$ ) until saturation. Subsequently, to eliminate weakly physically adsorbed  $\text{O}_2$  (or  $\text{C}_2\text{H}_4$ ) from the surface of the test sample, the gas flow was switched to pure He at a rate of 30 mL/min and maintained for another hour. Finally, the temperature was gradually increased to 900°C at a rate of 10°C /min to initiate the desorption process. During this stage, the signals of the desorbed gases were captured and analyzed using a mass spectrometer.

Acid-base titration analysis was used to measure the total content of silanol groups on the surface of silica. (Wang et al., 2015) Firstly, 25 ml ethanol and 75 ml NaCl solution (20 wt%) were added into the conical flask; Then, 1 g pre-dried silica (pre-drying temperature: 110 °C) was added, and the flask was sealed tightly before being vigorously shaken to ensure uniform mixing. The mixture was then allowed to equilibrate for 24 h to facilitate the interaction between the silica and the solution. To maintain a pH of 4 within the conical flask, 0.01 mol/L hydrochloric acid was carefully titrated into the solution. Following this, a basic burette filled with  $V_1$  ml of 0.01 mol/L ( $\text{C}_{\text{NaOH}}$ ) NaOH solution was then used to incrementally adjust the pH of the solution from 4 to 9. This adjustment was held for a minimum of 20 s to ensure stability. At the end of this step, the volume of NaOH in the basic burette was denoted as  $V_2$ . Utilizing formula (1), the silicon hydroxyl content ( $M$ , mmol/g) on the surface of the silica could be calculated.

$$M = \frac{C_{\text{NaOH}} \times (V_1 - V_2)}{m_{\text{SiO}_2}} \times 100\% \quad (1)$$

The Fourier transform infrared (FTIR) spectra were collected using a Nicolet-380 spectrometer equipped with a MCT detector. Experimental samples were compressed into self-supporting wafers and mounted in an *in situ* reaction cell. Prior to measurement, the wafers were pretreated through dehydration at 400 °C under nitrogen flow (30 mL/min) for 30 min to remove physisorbed water. After cooling to room temperature, the spectra were recorded. For the *in situ* FTIR study of EO conversion, the dehydrated catalyst was exposed to a 0.5 % EO gas mixture (balanced with N<sub>2</sub>) under continuous flow (30 mL/min) at 200 °C. Time-resolved infrared spectra were collected throughout the gas exposure period, with the background spectrum recorded under identical thermal conditions at 200 °C prior to EO introduction.

*In situ* Raman spectroscopy was conducted on a Horiba LabRAM HR evolution system to probe surface species on Ag particles. Prior to reaction, the catalyst was subjected to a reduction pretreatment under flowing H<sub>2</sub>/N<sub>2</sub> (1:4) at 350 °C for 2 h. Subsequently, the system was cooled to 50 °C under inert atmosphere, followed by acquisition of baseline Raman spectra. The pretreated catalyst was exposed to an O<sub>2</sub>/N<sub>2</sub> (1:9) mixture with temperature-programmed heating to 200 °C. *In situ* Raman spectra were recorded at key thermal stages (50 °C, 100 °C, 150 °C, and 200 °C), with the system held for 20 min at each temperature to ensure thermal equilibration. At 200 °C, the feed gas was switched to O<sub>2</sub>/C<sub>2</sub>H<sub>4</sub>/N<sub>2</sub> (3:1:6) to initiate ethylene epoxidation. Time-resolved Raman spectra were continuously acquired over 30 min under

isothermal conditions (200 °C) to track dynamic surface species evolution during catalysis.

#### 2.4. Catalysis test

The performance of catalysts was evaluated in a fixed bed reactor, employing a quartz tube with an inner diameter of 10 mm and a length of 450 mm as the reaction tube. The reduced Ag/SiO<sub>2</sub> catalyst (0.7 g, 20–40 mesh) was cooled to reaction temperature (200 °C), and a mixture of reactant gas (C<sub>2</sub>H<sub>4</sub>: O<sub>2</sub>: N<sub>2</sub> = 10: 30: 60) was introduced. The reaction proceeded under atmospheric pressure with a GHSV of 5657 mL/g/h. The products analysis was carried out using an Agilent 7890B gas chromatograph equipped with HP-PLOT/Q, MolSieve 5A, and Porapak Q column, complemented by both thermal conductivity detector (TCD) and flame ionization detector (FID). The experiment of ethylene oxide conversion on SiO<sub>2</sub> and Ag/SiO<sub>2</sub> catalysts was carried out at a temperature of 200 °C, with an EO standard gas (EO/N<sub>2</sub> = 0.5/99.5) flow of 1200 mL/g/h and 5657 mL/g/h respectively.

### 3. Results and discussion

#### 3.1. Characterization and quantitative analysis of surface Si-OH species

The SiO<sub>2</sub> support with abundant surface hydroxyl groups was first calcined at varying temperatures (500–800 °C) to systematically modulate the concentration and configuration of surface silanol species. (Sot et al., 2019) Subsequently, silver was loaded on the untreated/thermally

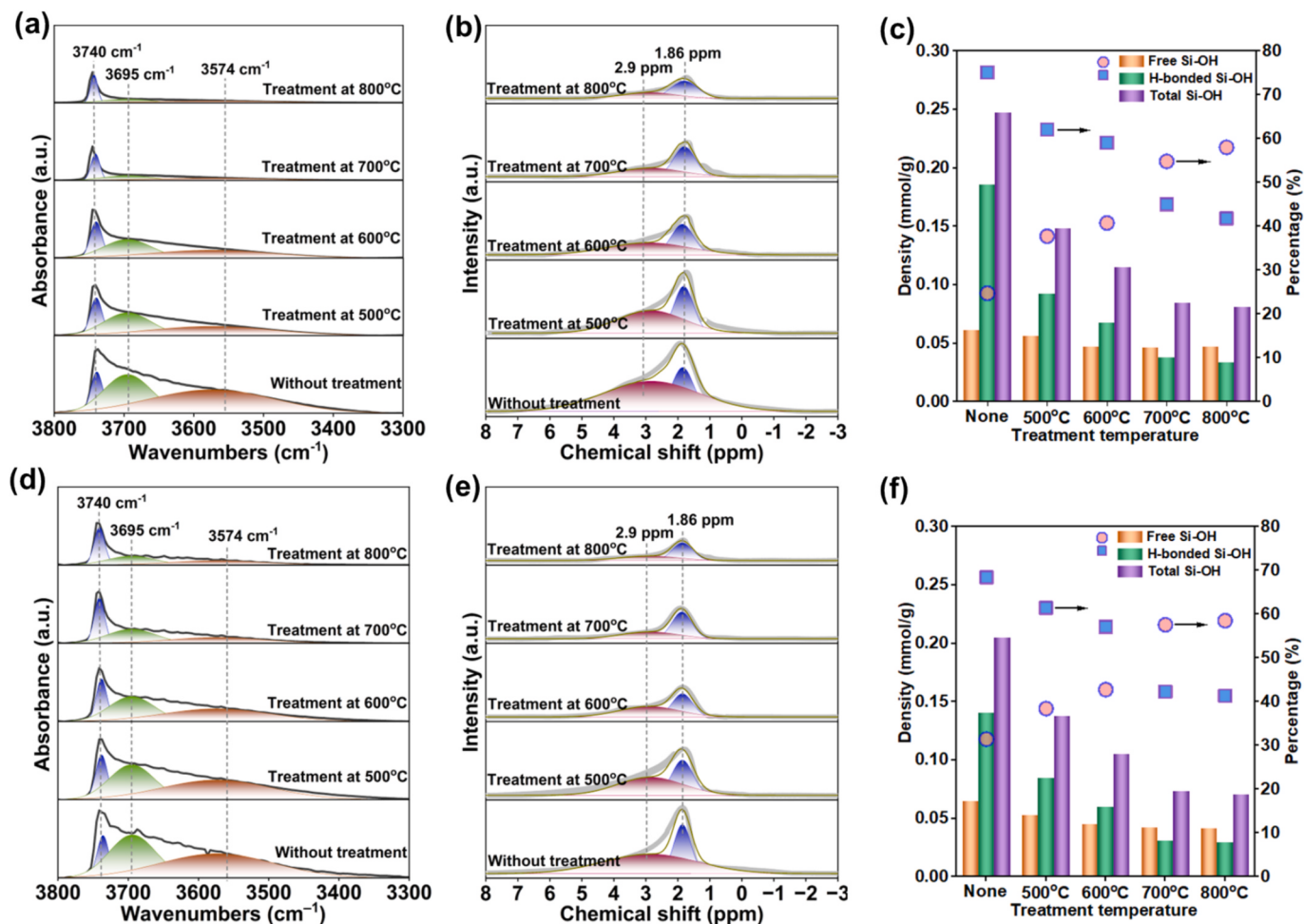


Fig. 1. Characterization and quantitative analysis of surface Si-OH species by employing *in situ* FTIR, <sup>1</sup>H NMR and chemical titration method. (a, b, c) pristine SiO<sub>2</sub> support samples treated at different calcination temperature. (d, e, f) Ag/SiO<sub>2</sub> catalyst series prepared using the corresponding SiO<sub>2</sub> support after treatment.

treated  $\text{SiO}_2$  supports through equal volume impregnation method, fabricating  $\text{Ag}/\text{SiO}_2$  catalysts with silver loading of 15 wt%. Characterization and quantitative analysis of surface Si-OH species were conducted by employing FTIR,  $^1\text{H}$  NMR and chemical titration method. Silanol species are typically identified by the O-H stretching vibration frequencies in infrared spectroscopy, with isolated silanols exhibiting an infrared stretching frequency of approximately  $3745 \text{ cm}^{-1}$  and hydrogen-bonded silanols displaying frequencies ranging from  $3715$  to  $3540 \text{ cm}^{-1}$ . (Dib et al., 2021; Paukshits et al., 2019; Mori et al., 2002; Cornac et al., 1984) FTIR spectra in Fig. 1a illustrates that the infrared peaks corresponding to surface silanol groups diminish dramatically with increasing heat treatment temperature, particularly those associated with hydrogen-bonded silanols. This was further confirmed by  $^1\text{H}$  NMR spectra from Fig. 1b. According to the literature, the chemical shift at 1.86 ppm corresponds to isolated silanol species, whereas the peak at 2.9 ppm is attributed to hydrogen-bonded silanol species. (Qu et al., 2005; Dubray et al., 2022) Deconvolution analysis reveals that as the heat treatment temperature of the  $\text{SiO}_2$  support increases, the reduction in hydrogen-bonded silanols exceeds that of isolated silanols, leading to a gradual increase in the proportion of isolated silanols. Specifically, the proportion of hydrogen-bonded silanols declined from 75.1 % to 40.52 %, whereas isolated silanols rose from 24.83 % to 59.48 %. Titration methods were employed to quantify the silanol species on the  $\text{SiO}_2$  surface (Wang et al., 2015; Lin et al., 2009; Kang et al., 2001). Combining the ratios derived from  $^1\text{H}$  NMR spectra, the quantities of each silanol type were calculated, as detailed in Fig. 1c. Thermal treatment at  $800^\circ\text{C}$  induced a 3.1-fold reduction in total silanol content from 0.25 mmol/g to 0.08 mmol/g. This overall decrease primarily originated from hydrogen-bonded silanol elimination, while isolated

silanol species exhibited minimal reduction (0.061 to 0.047 mmol/g). Strikingly, hydrogen-bonded silanols demonstrated a 5.5-fold depletion from 0.186 mmol/g to 0.034 mmol/g, suggesting their much higher thermal sensitivity. A similar trend is observed for  $\text{Ag}/\text{SiO}_2$  catalysts (Fig. 1d-f), indicating that the loading of silver does not significantly alter the concentration and distribution of silanols on the surface of the  $\text{SiO}_2$  support.

### 3.2. Characterization of morphology and texture properties

Scanning electron microscopy (SEM) and transmission electron microscopy (TEM) analyses were conducted on  $\text{SiO}_2$  samples treated at different temperatures and the corresponding  $\text{Ag}/\text{SiO}_2$  catalysts. As shown in Fig. 1a, there is no significant change in the morphology of  $\text{SiO}_2$  with increasing heat treatment temperature. The particles predominantly exhibit a spherical shape with an average size of approximately 50 nm. TEM results of  $\text{Ag}/\text{SiO}_2$  catalysts reveal ultrasmall silver particles (ca. 1.5–5.5 nm) on the  $\text{SiO}_2$  support, with a slight increase in silver particle size across samples prepared with  $\text{SiO}_2$  treated at enhanced temperatures. This trend is consistent with the enhanced peak intensity observed in the X-ray diffraction (XRD) patterns shown in Fig. 2b.  $N_2$  physisorption analysis was employed to investigate the textural properties of both supports and corresponding catalysts. As shown in Fig. 2c, the  $N_2$  adsorption–desorption isotherms of  $\text{SiO}_2$  carriers treated at different temperatures and their derived  $\text{Ag}/\text{SiO}_2$  catalysts all exhibited type IV characteristics with H3-type hysteresis loops in the  $P/P_0$  range of 0.9–1.0. The pore size distribution profiles (Fig. S1) revealed broad hierarchical porous architectures spanning 0–150 nm with irregular pore geometries. Quantitative analysis using BET and BJH

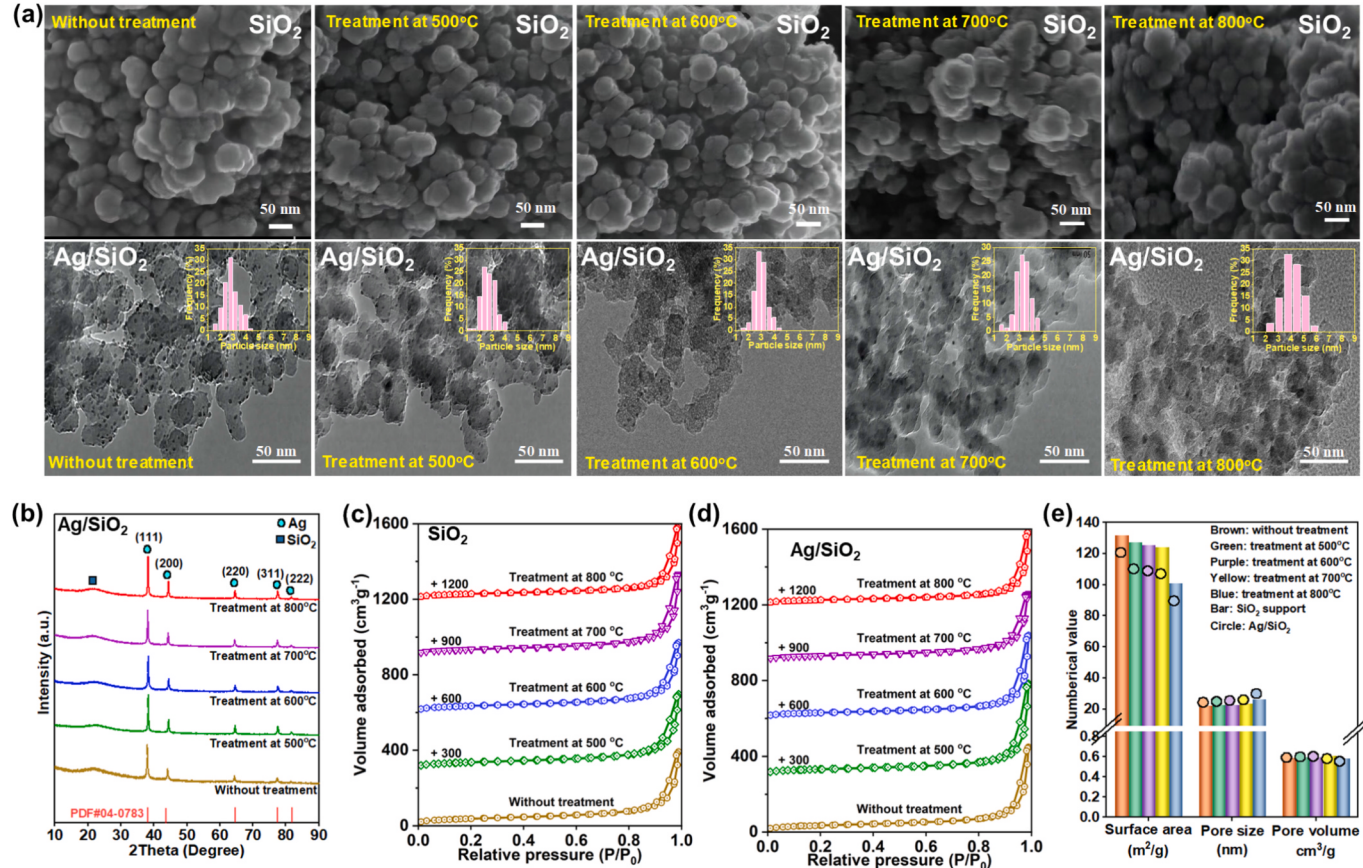


**Fig. 2.** Physicochemical properties characterizations of pristine  $\text{SiO}_2$  support and  $\text{Ag}/\text{SiO}_2$  catalysts. (a) Micro-morphological of pristine  $\text{SiO}_2$  supports (SEM images) treated at different calcination temperature and  $\text{Ag}/\text{SiO}_2$  catalysts (TEM images) prepared using the corresponding  $\text{SiO}_2$  support after treatment. (b) XRD patterns of  $\text{Ag}/\text{SiO}_2$  catalysts. (c-e) Textural structure information of  $\text{SiO}_2$  support and  $\text{Ag}/\text{SiO}_2$  catalysts obtained from physical  $N_2$  adsorption and desorption isotherms.

models demonstrated comparable textural parameters (specific surface area, pore volume, average pore diameter, and pore size distribution) for  $\text{SiO}_2$  supports and  $\text{Ag}/\text{SiO}_2$  catalysts treated below 700 °C, respectively (Fig. 2e, Fig. S1). However, thermal treatment at 800 °C seemingly induced sintering effects, manifested by obvious reduction in surface area and increase in average pore diameter.

### 3.3. Physicochemical properties characterizations of $\text{Ag}/\text{SiO}_2$ catalysts

XPS analysis confirms the predominant presence of metallic silver ( $\text{Ag}^0$ ) across all  $\text{Ag}/\text{SiO}_2$  catalysts, with consistent electronic states observed regardless of support pretreatment conditions (Fig. 3a). The oxygen temperature programmed oxidation ( $\text{O}_2\text{-TPO}$ ) characterization of  $\text{Ag}/\text{SiO}_2$  catalysts demonstrates distinct oxidation behavior variations depending on  $\text{SiO}_2$  support pretreatment temperatures. Elevating the support pretreatment temperature induces a concomitant reduction in oxygen adsorption capacity, although similar oxidation temperatures are observed for catalysts with supports pretreated at  $\leq 700$  °C. This behavior likely originates from the growth of silver particles (evidenced by TEM and XRD analysis). Notably, at 800 °C pretreatment, the catalysts exhibit a pronounced low-temperature shift ( $\sim 25$  °C) in their TCD response profiles. This should be related to highly strained four-membered siloxane rings on the silica material formed at high temperatures (when reaching 800 °C), (Scott and Basset, 1994; Bunker et al.,

1989) which may affect the electronic properties of the supported Ag particles.

To elucidate the nature of oxygen species on silver particles, spectroscopic investigations were conducted. Fig. 3e-f presents the temperature-dependent *in situ* Raman spectra of  $\text{O}_2$ -oxidized  $\text{Ag}/\text{SiO}_2$  catalysts under flowing  $\text{O}_2$  atmosphere across a temperature range of 50–200 °C. The results reveal that both hydrogen-bonded silanol rich  $\text{Ag}/\text{SiO}_2$  and nearly hydrogen-bonded silanol free samples exhibit a prominent oxygen species-related peak centered around 800 cm<sup>-1</sup>, which should be assigned to dioxygen complexes ( $\text{O}_2^*$ ), (Liu et al., 2022; Chen et al., 2025; Pu et al., 2023) and showing greater thermal stability at lower temperatures as the peak intensity progressively diminishes with increasing temperature. Most recently, Jalil reported that nickel (Ni) as a dopant in Ag that can facilitate selective oxidation by activating molecular oxygen ( $\text{O}_2$ ) without binding oxygen (O) too strongly, indicating a strong correlation between desorption ability of O species and EO selectivity. (Jalil et al., 2025) In our work, temperature programmed desorption of oxygen ( $\text{O}_2\text{-TPD}$ ) analysis for  $\text{Ag}/\text{SiO}_2$  catalysts with different surface Si-OH species was also conducted to elucidate the silver-oxygen interaction dynamics influenced by silanol. The TPD profile of the catalyst pre-oxidized at 50 °C exhibits two characteristic desorption peaks. While all samples demonstrate a low-temperature desorption peak around 200 °C, those containing hydrogen-bonded silanol groups reveal an additional prominent high-temperature peak

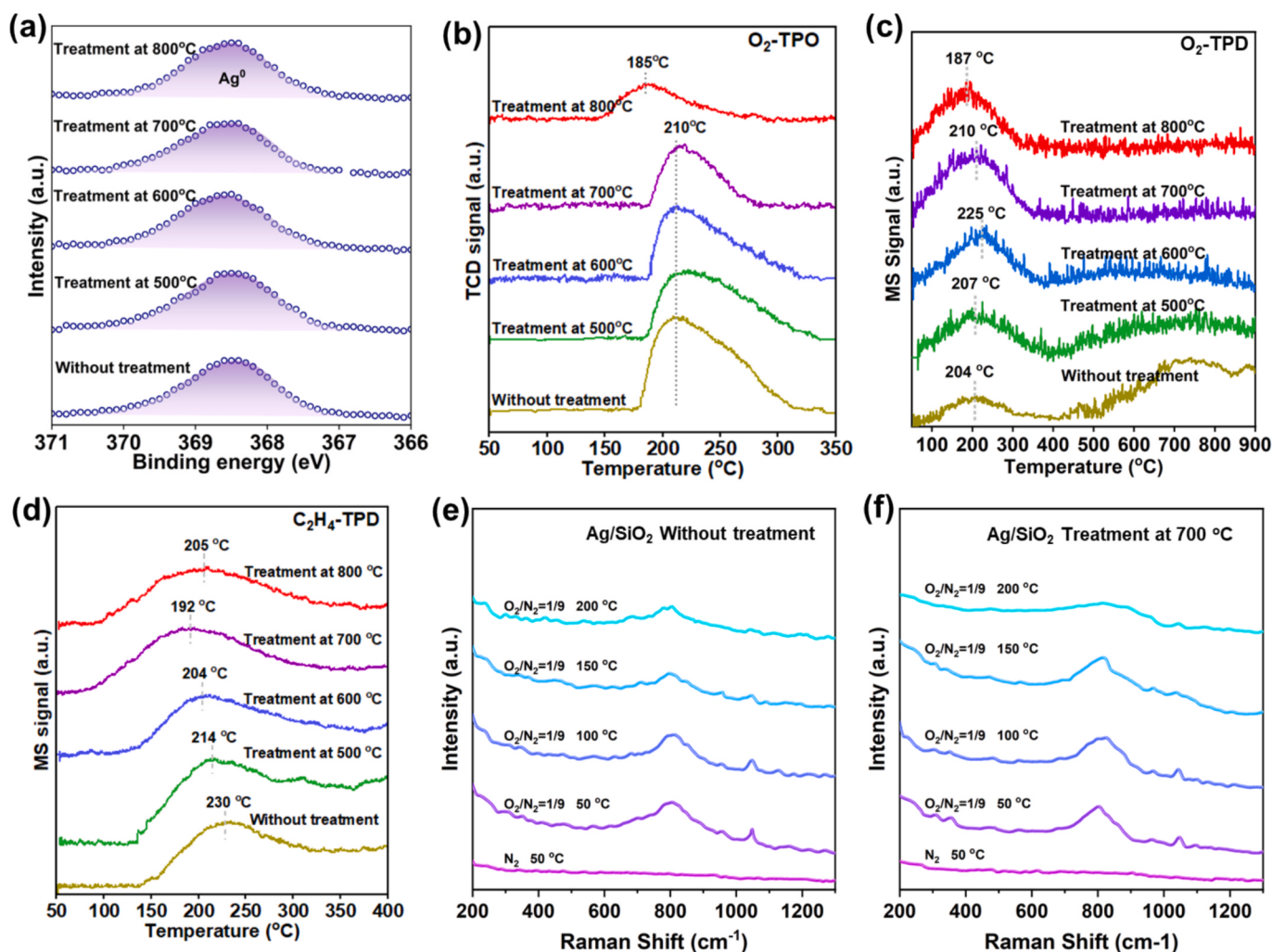


**Fig. 3.** Physicochemical properties characterizations of  $\text{Ag}/\text{SiO}_2$  catalysts. (a) XPS Ag 3d spectra, (b)  $\text{O}_2\text{-TPO}$ , (c)  $\text{O}_2\text{-TPD}$ , and (d)  $\text{C}_2\text{H}_4\text{-TPD}$  of reduced  $\text{Ag}/\text{SiO}_2$  catalysts prepared using  $\text{SiO}_2$  support after treatment at different calcination temperature. (e-f) *In situ* Raman spectra of temperature-programmed oxidation (50 – 200 °C, spectra every 50 °C). The reduction of catalyst is conducted in 30 mL/min 10 % $\text{H}_2/\text{He}$  flow at 350 °C for 2 h.

(>500 °C). Notably, the Ag/SiO<sub>2</sub> catalyst with untreated support displays the most intensive high-temperature desorption feature. Nagy et al. and Bao et al. have assigned this peak to subsurface oxygen (O<sub>y</sub>) that diffuses via an interstitial diffusion mechanism. (Qu et al., 2005; Zhang et al., 2016; Nagy et al., 1999) It is noteworthy that this peak is prominently observed on silica-supported silver catalysts, while very weak on polycrystalline silver foil. (Qu et al., 2005; Zhang et al., 2016; Nagy et al., 1999) However, this O<sub>y</sub> desorption peak in our work gradually diminishes with the reduction of hydrogen-bonded silanol groups in the samples, and is almost undetectable in the sample treated at

700 °C (hydrogen-bonded silanol groups are effectively reduced). This suggests that there should be an interfacial interaction between the silanol groups and the silver particles or clusters, which could potentially influence the electronic characteristics of the silver and the desorption behavior of surface species.

Intriguingly, this “silanol-mediated” effect also significantly influences ethylene desorption behavior, as evidenced by the temperature programmed desorption of ethylene (C<sub>2</sub>H<sub>4</sub>-TPD) profiles in Fig. 3d. With progressive depletion of hydrogen-bonded silanol groups on the catalyst surface, the ethylene desorption peak systematically shifts toward lower

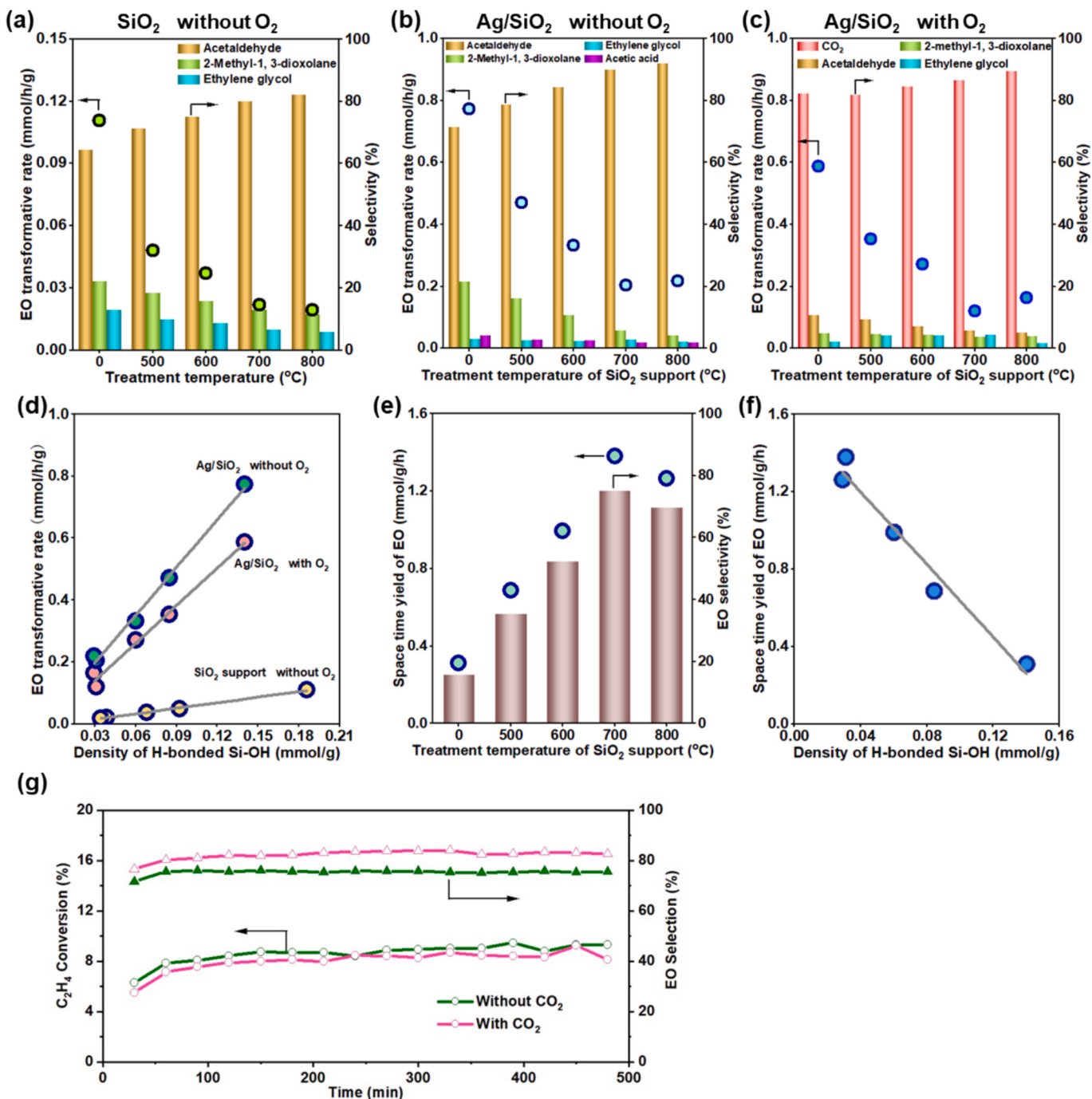


**Fig. 4.** Effect of treatment temperature of SiO<sub>2</sub> support on the EO transformation and by-products distribution over (a) SiO<sub>2</sub> support and Ag/SiO<sub>2</sub> catalysts (b) without and (c) with oxygen. (d) Relationship between the density of H-bonded Si-OH group and EO transformation on SiO<sub>2</sub> support and Ag/SiO<sub>2</sub> catalysts. (e) Effect of treatment temperature of SiO<sub>2</sub> support on the space time yield of EO in ethylene epoxidation over Ag/SiO<sub>2</sub> catalysts. (f) Correlation between the density of H-bonded Si-OH group and space time yield of EO on Ag/SiO<sub>2</sub> catalysts. (g) Catalytic stability test at 200 °C at a space time of 5657 mL/g/h (without CO<sub>2</sub>: C<sub>2</sub>H<sub>4</sub>/O<sub>2</sub>/N<sub>2</sub> = 1/3/6, with CO<sub>2</sub>: CO<sub>2</sub>/C<sub>2</sub>H<sub>4</sub>/O<sub>2</sub>/N<sub>2</sub> = 0.15/1/3/5.85).

temperatures, reaching its minimum desorption temperature on the 700 °C treated sample. However, a counterintuitive reversal emerges upon further increasing the pretreatment temperature to 800 °C, where the desorption peak shifts back toward higher temperatures. This non-monotonic thermal response implies the formation of distinct surface species at elevated temperatures, which may induce electronic or structural modifications to silver nanoparticles, thereby altering their interaction dynamics with ethylene.

### 3.4. Reaction performance of ethylene epoxidation and EO transformation

The effect of SiO<sub>2</sub> supports treated at different temperatures and corresponding Ag/SiO<sub>2</sub> catalysts on the transformation of EO was investigated. For SiO<sub>2</sub> without silver loading (Fig. 4a), the EO conversion rate decreased from 0.11 mmol/g/h (untreated) to 0.02 mmol/g/h (treated at 800 °C) with the decreasing of the density of H-bonded Si-OH group, representing a nearly sixfold reduction. The primary product of EO conversion was acetaldehyde, with minor products including 2-methyl-1,3-dioxolane and ethylene glycol (Confirmed by mass spectrometry, Fig. S2). Additionally, the EO decomposition performance of Ag/SiO<sub>2</sub> catalysts with SiO<sub>2</sub> supports pretreated at different temperatures was also evaluated. As shown in Fig. 4b, the presence of Ag significantly amplified the transformation capability of EO compared to the unsupported SiO<sub>2</sub> case. For the untreated Ag/SiO<sub>2</sub> catalyst, the conversion rate of EO reaches as high as 0.77 mmol/g<sub>cat</sub>/h, indicating that Ag particles formed on SiO<sub>2</sub> support play a significant role in EO conversion. The EO conversion rate over Ag/SiO<sub>2</sub> catalysts decreased significantly from 0.77 mmol/g/h to 0.20 mmol/g/h as the pretreatment temperature of the SiO<sub>2</sub> support increased to 700 °C. A similar trend was observed in the presence of oxygen, except for that acetaldehyde underwent further oxidation to form CO<sub>2</sub> (Fig. 4c). (Miller et al., 2020) However, when the SiO<sub>2</sub> support was pretreated at 800 °C, the EO conversion rate slightly increased to 0.22 mmol/g/h. This may be also related to high-strain four-membered siloxane rings generated at 800 °C (evidenced by TPO and TPD results). (Scott and Bassett, 1994; Dubois and Zegarski, 1993) The correlation between the hydrogen-bonded silanol content of the samples and the conversion rate of EO is illustrated in Fig. 4d. The results demonstrate a nearly linear relationship between the quantity of hydrogen-bonded silanol species and the extent of EO conversion rate for both SiO<sub>2</sub> and Ag/SiO<sub>2</sub> catalysts, regardless of the presence of oxygen.

The performance of Ag/SiO<sub>2</sub> catalysts prepared from SiO<sub>2</sub> supports pretreated at different temperatures was evaluated for the ethylene epoxidation reaction, with the results shown in Fig. 4e and Fig. S3. The catalyst prepared using the untreated support exhibited a space time yield (STY) of EO as low as 0.31 mmol/g/h, with an EO selectivity of just 15.7 %. As the treatment temperature increased, the conversion of ethylene showed a slight decrease, while the selectivity to EO dramatically improved. At a 700 °C treated support, the STY reached 1.38 mmol/g/h, with an ethylene conversion of 7.3 % and an EO selectivity of 75.1 %. The significant improvement in the selectivity and yield of EO is inversely correlated with the sharp reduction in the quantity of silanol species on the catalyst surface, particularly hydrogen-bonded silanol species (Fig. 4f). When the support pretreatment temperature furtherly reaches 800 °C, the selectivity of EO over the Ag/SiO<sub>2</sub> catalyst decreases, likely related to the high-strain four-membered siloxane rings formed in the SiO<sub>2</sub> support. Fig. 4g illustrates that the catalyst with a support pretreated at 700°C exhibited excellent performance, maintaining an EO selectivity of approximately 75 % during 500 min of reaction, with negligible signs of deactivation. Furthermore, the introduction of CO<sub>2</sub> into the system enhanced EO selectivity to 81 % without causing a noticeable reduction in reaction activity (Fig. 4g, Fig. S4).

### 3.5. Spectroscopic study of ethylene epoxidation and EO transformation

Pu et al. have systematically studied oxygen species on Ag/αAl<sub>2</sub>O<sub>3</sub> using Raman spectroscopy and identified that silver–oxygen species formed on silver particle surfaces serve as the determining factor for ethylene epoxidation selectivity. (Pu et al., 2023; Pu et al., 2022) In this work, we employed *In situ* Raman spectroscopy to probe oxygen species evolution on silica-supported silver nanocatalysts during ethylene oxidation. The results revealed comparable surface oxygen species profiles between two distinct catalysts with markedly different catalytic performance (Figs. 5a, d). Both samples displayed a predominant characteristic peak at ~ 800 cm<sup>-1</sup>, which was identified as diatomic oxygen configurations (O<sub>2</sub><sup>\*</sup>). (Liu et al., 2022; Chen et al., 2025; Pu et al., 2023) Chen et al. (Chen et al., 2025) reported that the O<sub>2</sub><sup>\*</sup> species, which tends to form under higher O<sub>2</sub> pressures and oxygen coverages, plays a pivotal role in facilitating the selective formation of EO. However, the O<sub>1</sub><sup>\*</sup> species with a peak position around 350 cm<sup>-1</sup> tends to induce C-C bond cleavage or deep oxidation, leading to the formation of carbon dioxide (CO<sub>2</sub>). This unique feature on Ag/SiO<sub>2</sub> (with O<sub>2</sub><sup>\*</sup> as a dominant species) potentially originates from the silica support's influence on silver particle properties, accounting for the exceptional 80 % EO selectivity achieved in our catalyst system without additional promoters. These findings suggest that silica-supported silver catalysts may possess certain intrinsic benefits for ethylene epoxidation. Specifically, the silica substrate appears to influence the electronic properties of silver, thereby stabilizing key oxygen intermediates. However, this potential advantage has historically been overshadowed by challenges in controlling secondary ethylene oxide conversion on the support surface.

To elucidate the mechanistic details of EO secondary conversion during ethylene epoxidation, we performed *in situ* FTIR to monitor EO decomposition on catalyst surfaces. As illustrated in Fig. 5b, exposure of untreated silica support to EO shows a complex array of surface intermediates, with spectral features systematically assigned based on established vibrational signatures. (Bulushev et al., 1995) The weak bands at 3065 and 3005 cm<sup>-1</sup> correspond to vibrations of CH<sub>2</sub> belonging to EO. (Xiong et al., 2021) The broad absorption spanning 3200–3600 cm<sup>-1</sup> originates from hydroxyl groups participating in hydrogen-bond interactions, critical for stabilizing adsorbed species, while the bands at 2885 and 2950 cm<sup>-1</sup> should be attributed to the stretching CH vibrations of CH<sub>2</sub> and CH<sub>3</sub> fragments belonging to surface species. The peaks of these surface species can also be observed on low hydroxyl SiO<sub>2</sub> (Fig. 5e), but significantly weakened. The coexistence of these intermediates highlights the competition between EO stabilization and decomposition on silica surfaces, with the hydroxyl species at 3400 cm<sup>-1</sup> likely serving as pivotal intermediates governing both EO retention and subsequent secondary conversion events. Based on the experimental observations and relevant literature reports, we propose that the glycol-like surface species (−OCH<sub>2</sub>CH<sub>2</sub>OH) serves as the key intermediate in the conversion of EO on hydrogen-bonded silanol. (Bulushev et al., 1995) As shown in Fig. S5; this intermediate may undergo subsequent transformations through three possible pathways: (1) hydrogen transfer to form acetaldehyde as the primary byproduct, (2) reaction with another EO molecule or acetaldehyde to generate 2-methyl-1,3-dioxolane, or (3) hydrolysis with environmental water molecules to produce ethylene glycol.

The characteristic band at 1620 cm<sup>-1</sup>, corresponding to the asymmetric stretching vibrations of surface carboxylates (−COO), exhibited remarkable enhancement on Ag/SiO<sub>2</sub> catalysts (Fig. 5c) compared to SiO<sub>2</sub> (Fig. 5b). However, comparable intensities of carboxylate species were observed on both high and low hydrogen-bonded silanol samples after silver loading (Fig. 5c f). This suggests that the dramatic difference in EO conversion capability between the two catalysts originates from their silanol characteristics rather than silver species variations. Interestingly, FTIR spectra show a significant reduction in the hydroxyl (3400 cm<sup>-1</sup>) and CH<sub>2</sub> and CH<sub>3</sub> (2885 and 2950 cm<sup>-1</sup>) related to −OCH<sub>2</sub>CH<sub>2</sub>OH surface species on Ag/SiO<sub>2</sub> catalysts (Fig. 5c f) compared

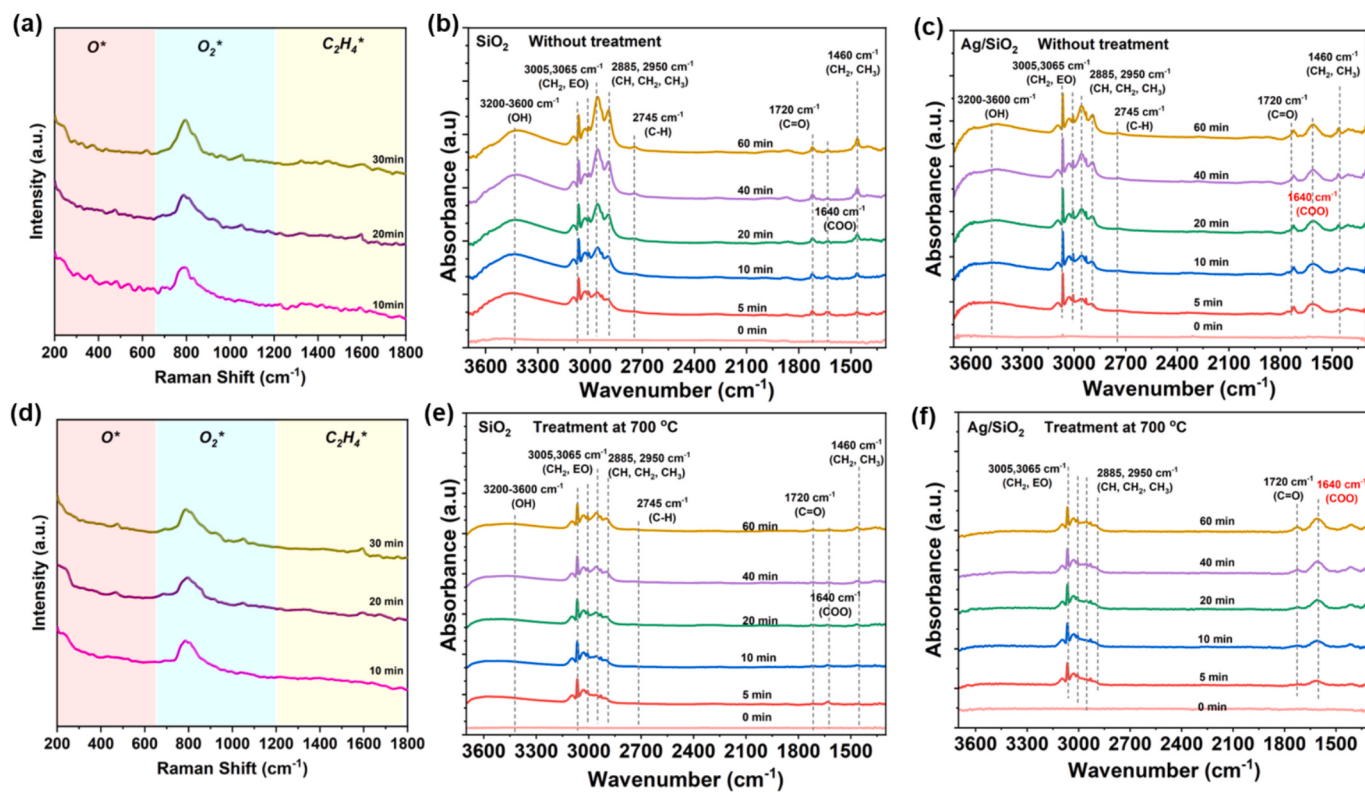


**Fig. 5.** (a) *In situ* Raman spectra of silver–oxygen species during the ethylene–oxygen reaction over the Ag/SiO<sub>2</sub> catalyst with untreated SiO<sub>2</sub>. *In situ* FTIR spectra of EO conversion on (b) untreated SiO<sub>2</sub> and (c) the corresponding Ag/SiO<sub>2</sub> catalyst; (d) *In situ* Raman spectra of silver–oxygen species during the ethylene–oxygen reaction over Ag/SiO<sub>2</sub> catalyst with SiO<sub>2</sub> pretreated at 700 °C. *In situ* FTIR spectra of EO conversion on (e) SiO<sub>2</sub> treated at 700 °C and (f) corresponding Ag/SiO<sub>2</sub> catalyst. All spectroscopic measurements were conducted at 200 °C.

to SiO<sub>2</sub> supports (Fig. 5b e), although silver loading dramatically enhanced the secondary conversion capacity of EO. This apparent contradiction indicates that the introduced silver species facilitate rapid transformation and desorption of the glycol-like surface intermediates ( $-OCH_2CH_2OH$ ), leading to the formation of final products including acetaldehyde, 2-methyl-1,3-dioxolane, and ethylene glycol, thereby achieving the observed magnitude enhancement in EO conversion efficiency after silver modification.

### 3.6. Kinetic insights into ethylene epoxidation over Ag/SiO<sub>2</sub>

A systematic kinetic investigation was conducted to elucidate the ethylene epoxidation behavior over Ag/SiO<sub>2</sub> catalysts with varying hydrogen-bonded silanol densities. Prior to kinetic measurements, rigorous validation experiments confirmed the elimination of internal and external diffusion limitations. The reaction order of ethylene (or oxygen) is determined by varying the concentration of ethylene (or oxygen) while keeping the oxygen (or ethylene) concentration constant at a substantial excess. The obtained relationship between the generation rate of the product (EO/CO<sub>2</sub>) and the concentration of the reactants

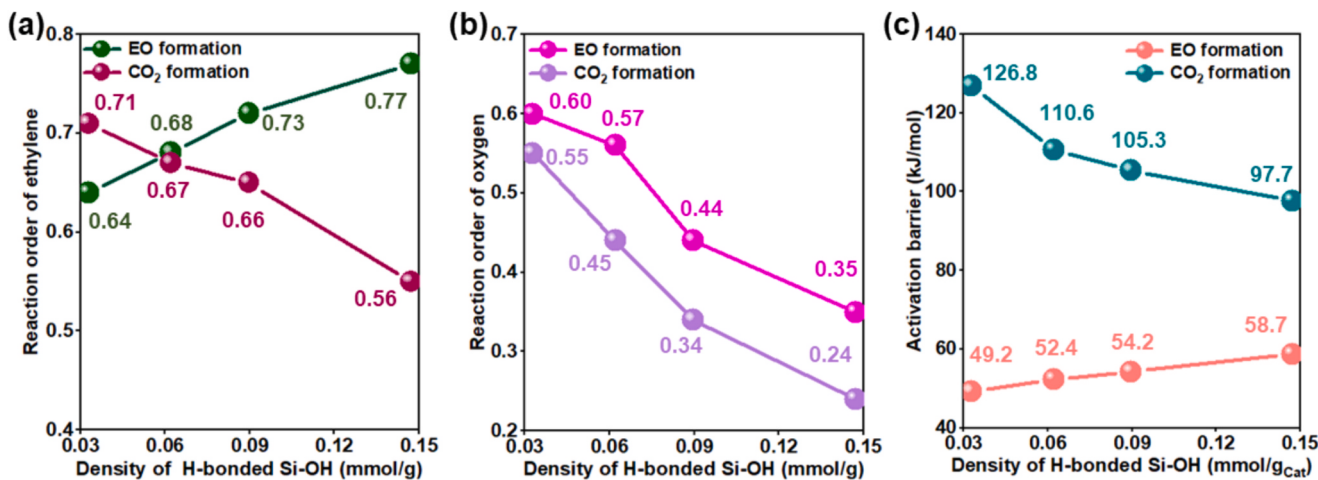


**Fig. 6.** Kinetic insights into ethylene epoxidation. Effect of H-bonded Si-OH group density on the reaction order of (a) ethylene and (b) oxygen and (c) activation barrier for EO formation and ethylene over-oxidation.

(ethylene/oxygen) is shown in the Fig. S6. Further analysis revealed critical structure–activity relationships between silanol density and kinetic parameters. Fig. 6a demonstrates that increasing hydrogen-bonded silanol content enhances the ethylene reaction order for EO formation, while simultaneously diminishing its influence on CO<sub>2</sub> production. Conversely, Fig. 6b illustrates an inverse correlation between silanol density and oxygen reaction orders for both pathways (EO and CO<sub>2</sub>), indicating a reduced impact of oxygen concentration on the reaction rates of these processes.

Temperature-dependent studies (195–215°C, Fig. S7) enabled determination of Arrhenius parameters. Fig. 6c establishes a direct proportionality between silanol density and apparent activation energies: the apparent activation energy for EO increases systematically with silanol content, whereas exhibiting an inverse trend for CO<sub>2</sub>. This energetic decoupling mechanism explains the enhanced EO selectivity observed in hydrogen-bonded silanol depleted catalysts. Consequently, minimizing the number of hydrogen-bonded silanol species is critical when employing high surface area SiO<sub>2</sub> as a support for silver catalysts in ethylene epoxidation.

#### 4. Conclusion

In this study, Ag/SiO<sub>2</sub> catalysts with nano-sized silver supported on high-surface-area silica were synthesized and systematically investigated for ethylene epoxidation. Our findings highlight the crucial role of hydrogen-bonded silanol species in governing the catalytic performance of Ag/SiO<sub>2</sub>. These species significantly influence the isomerization of EO into acetaldehyde and other by-products, while also affecting the desorption kinetics of surface species on silver. Moreover, we confirm that O<sub>2</sub>\* is the predominant reactive oxygen species on the Ag surface and that hydrogen-bonded silanols substantially hinder the desorption of surface oxygen species, thereby potentially impacting the overall epoxidation process. Additionally, these silanols promote the formation of glycol-like intermediates from EO, and their interaction with silver species facilitates the transformation and desorption of these intermediates, further accelerating the secondary conversion of EO. Kinetic analysis reveals that reducing hydrogen-bonded silanol content lowers the activation energy for EO formation while increasing it for deep oxidation reactions. High-temperature treatment of the silica support effectively diminishes hydrogen-bonded silanol species, thereby enhancing EO selectivity. As a result, thermal pre-treatment of the support improves catalyst selectivity to 81 %, primarily by reducing the density of hydrogen-bonded silanol groups.

#### CRediT authorship contribution statement

**Kaipeng Cao:** Writing – original draft, Investigation, Formal analysis, Data curation. **Min Huang:** Software, Investigation, Formal analysis. **Gang Wang:** Writing – review & editing, Formal analysis. **Jie Li:** Writing – review & editing, Formal analysis. **Chunshan Li:** Writing – review & editing, Project administration, Funding acquisition, Conceptualization.

#### Declaration of competing interest

The authors declare that they have no known competing financial interests or personal relationships that could have appeared to influence the work reported in this paper.

#### Acknowledgments

This work is supported by the National Natural Science Fund for Distinguished Young Scholars (Grant 22025803), and funding from Zhongke-Yuneng Joint R&D Center.

#### Data availability

Data will be made available on request.

#### References

- Pu, T., Tian, H., Ford, M.E., Rangarajan, S., Wachs, I.E., 2019. Overview of selective oxidation of ethylene to ethylene oxide by Ag catalysts. *ACS Catal.* 9, 10727–10750.
- Chu, Y., Liang, H., Lin, Q., Huang, H., Che, P., Han, Y., 2025. Effect of water vapor on the structure and performance of silver catalysts for ethylene oxidation. *Chem. Eng. J.* 518, 146994.
- Soni, Y., March, S., Suib, S.L., Sykes, E.C.H., Deshlahra, P., 2025. Structure and reactivity of AgCu/SiO<sub>2</sub> bimetallic catalysts for alkene epoxidation. *ChemCatChem* e202500123.
- Hus, M., Grilc, M., Terzan, J., Gyergyek, S., Likozar, B., Hellman, A., 2023. Going beyond silver in ethylene epoxidation with first-principles catalyst screening. *Angew. Chem. Int. Ed.* 62, e202218456.
- Hwang, A., Klaucke, J., Lizandara-Pueyo, C., Karpov, A., Iglesia, E., 2024. Roles of Re and Cs promoters and organochlorine moderators in the synthesis of ethylene oxide on Ag-based catalysts. *ChemCatChem* 16, e202400111.
- Christopher, P., Linic, S., 2008. Engineering selectivity in heterogeneous catalysis: Ag nanowires as selective ethylene epoxidation catalysts. *J. Am. Chem. Soc.* 130, 11264–11265.
- Hus, M., Hellman, A., 2019. Ethylene epoxidation on Ag(100), Ag(110), and Ag(111): a joint ab initio and kinetic Monte Carlo study and comparison with experiments. *ACS Catal.* 9, 1183–1196.
- Guo, M., Dongfang, N., Iannuzzi, M., van Bokhoven, J.A., Artiglia, L., 2024. Structure and reactivity of active oxygen species on silver surfaces for ethylene epoxidation. *ACS Catal.* 14, 10234–10244.
- van Santen, R.A., Kuipers, H., 1987. The mechanism of ethylene epoxidation. *Adv. Catal.* 35, 265–321.
- Jalil, A., Happel, E.E., Cramer, L., Hunt, A., Hoffman, A.S., Waluyo, I., Montemore, M.M., Christopher, P., Sykes, E.C.H., 2025. Nickel promotes selective ethylene epoxidation on silver. *Science* 387, 869–873.
- Ramirez, A., Hueso, J.L., Suarez, H., Mallada, R., Ibarra, A., Irusta, S., Santamaría, J., 2016. A nanoarchitecture based on silver and copper oxide with an exceptional response in the chlorine-promoted epoxidation of ethylene. *Angew. Chem. Int. Ed.* 55, 11158–11161.
- Serafin, J.G., Liu, A.C., Seyedmonir, S.R., 1998. Surface science and the silver-catalyzed epoxidation of ethylene: an industrial perspective. *J. Mol. Catal. A Chem.* 131, 157–168.
- Diao, W., DiGiulio, C.D., Schaal, M.T., Ma, S., Monnier, J.R., 2015. An investigation on the role of Re as a promoter in Ag–Cs/Re– $\alpha$ -Al<sub>2</sub>O<sub>3</sub> high-selectivity ethylene epoxidation catalysts. *J. Catal.* 322, 14–23.
- Keijzer, C.J., Weide, P.T., Helfferich, K.H., Zieciak, J., de Ridder, M., Dalebout, R., Lohr, T.L., Lockemeyer, J.R., van den Brink, P., de Jongh, P.E., 2025. Insight into the influence of Re and Cl on Ag catalysts in ethylene epoxidation. *Cat. Sci. Technol.* 15, 323–333.
- Keijzer, C.J., van de Ven, N.M.T., Dalebout, R., Lohr, T.L., Lockemeyer, J.R., van den Brink, P., de Jongh, P.E., 2025. Influence of alkali and chloride promoters on silver catalysts in ethylene epoxidation. *J. Catal.* 450, 115592.
- Salaev, M.A., 2021. Computational insights into promoting effects of alkali metals, Re, and Cl for silver catalysts of ethylene epoxidation. *Mol. Catal.* 507, 111543.
- Keivanimehr, F., Mokhtari, M., Habibzadeh, S., 2025. Synergistic effect of Ag(111) and transition-metal promoters toward optimization of catalytic ethylene epoxidation selectivity. *Sci. Rep.* 15, 4567.
- Rocha, T.C.R., Haevecker, M., Knop-Gericke, A., Schlägl, R., 2014. Promoters in heterogeneous catalysis: the role of Cl on ethylene epoxidation over Ag. *J. Catal.* 312, 12–16.
- Pursell, D.P., Bocquet, M.L., Vohs, J.M., Dai, H.L., 2003. Adsorption structure, energetics, and thermal reactions of vinyl chloride on Ag(111). *Surf. Sci.* 522, 90–104.
- Campbell, C.T., Paffett, M.T., 1984. The role of chlorine promoters in catalytic ethylene epoxidation over the Ag(110) surface. *Appl. Surf. Sci.* 19, 28–42.
- Iyer, K.R., Bhan, A., 2024. The role of chlorine promoters in mediating particle-size effects in silver-catalyzed ethylene epoxidation. *J. Catal.* 436, 115451.
- Sun, L., Huang, H., Che, P., Lin, Q., Lian, K., Li, J., Zhang, Y., Han, Y., 2022. In-situ discovery on the formation of supported silver catalysts for ethylene epoxidation. *Adv. Powder Technol.* 33, 103478.
- van den Reijen, J.E., Kanungo, S., Welling, T.A.J., Versluijs-Helder, M., Nijhuis, T.A., de Jong, K.P., de Jongh, P.E., 2017. Preparation and particle-size effects of Ag/ $\alpha$ -Al<sub>2</sub>O<sub>3</sub> catalysts for ethylene epoxidation. *J. Catal.* 356, 65–74.
- Keijzer, C.J., Smulders, L.C.J., Wezendonk, D., de Rijk, J.W., de Jongh, P.E., 2024. Influence of Ag particle size and Ag:Al<sub>2</sub>O<sub>3</sub> surface ratio in catalysts for the chloride-promoted ethylene epoxidation. *Catal. Today* 428, 114120.
- Egelske, B.T., Xiong, W., Zhou, H., Monnier, J.R., 2022. Effects of the method of active-site characterization for determining structure-sensitivity in Ag-catalyzed ethylene epoxidation. *J. Catal.* 410, 221–235.
- van Hoof, A.J.F., Hermans, E.A.R., van Bavel, A.P., Friedrich, H., Hensen, E.J.M., 2019. Structure sensitivity of silver-catalyzed ethylene epoxidation. *ACS Catal.* 9, 9829–9839.
- Salaev, M.A., Salaeva, A.A., Vodyankina, O.V., 2021. Towards the understanding of promoting effects of Re, Cs and Cl promoters for silver catalysts of ethylene epoxidation: a computational study. *Catal. Today* 375, 585–590.

- Yong, Y.S., Kennedy, E.M., Cant, N.W., 1991. Oxide-catalyzed reactions of ethylene oxide under conditions relevant to ethylene epoxidation over supported silver. *Appl. Catal. 76*, 31–48.
- van den Reijen, J.E., Versluis, W.C., Kanungo, S., d'Angelo, M.F., de Jong, K.P., de Jongh, P.E., 2019. From qualitative to quantitative understanding of support effects on the selectivity in silver-catalyzed ethylene epoxidation. *Catal. Today 338*, 31–39.
- Kanoh, H., Nishimura, T., Ayame, A., 1979. Supported silver catalysts for the oxidation of ethylene—effects of thermal treatment of alumina as catalyst support. *J. Catal. 57*, 372–379.
- Jain, D., Stangland, E., 2025. A perspective on the role and development of supports for maximizing the efficiency of catalytic gas-phase ethylene epoxidation. *Energy Fuels 39*, 12309–12322.
- Fotopoulos, A.P., Triantafyllidis, K.S., 2007. Ethylene epoxidation on Ag catalysts supported on non-porous, microporous and mesoporous silicates. *Catal. Today 127*, 148–156.
- Lee, J.K., Verykios, X.E., Pitchai, R., 1988. Support participation in chemistry of ethylene oxidation on silver catalysts. *Appl. Catal. 44*, 223–237.
- Bulushev, D.A., Paukshtis, E.A., Nogin, Y.N., Balzhinimaev, B.S., 1995. Transient-response and infrared studies of ethylene-oxide reactions on silver catalysts and supports. *Appl. Catal. A 123*, 301–322.
- Mao, C.F., Vannice, M.A., 1995. High-surface-area  $\alpha$ -aluminas. III. Oxidation of ethylene, ethylene oxide, and acetaldehyde over silver dispersed on high-surface-area  $\alpha$ -alumina. *Appl. Catal. A 122*, 61–76.
- Wang, Y., He, M.Y., Chen, R.Y., 2015. Fabrication of mechanically robust antireflective films using silica nanoparticles with enhanced surface hydroxyl groups. *J. Mater. Chem. A 3*, 1609–1618.
- Sot, P., Copéret, C., van Bokhoven, J.A., 2019. Fully dehydroxylated silica generated from hydrosilane: surface defects and reactivity. *J. Phys. Chem. C 123*, 23480–23487.
- Dib, E., Costa, I.M., Vayssilov, G.N., Aleksandrov, H.A., Mintova, S., 2021. Complex H-bonded silanol network in zeolites revealed by IR and NMR spectroscopy combined with DFT calculations. *J. Mater. Chem. A 9*, 27347–27352.
- Paukshtis, E.A., Yaranova, M.A., Batueva, I.S., Balzhinimaev, B.S., 2019. A FTIR study of silanol nests over mesoporous silicate materials. *Microporous Mesoporous Mater. 288*, 109597.
- Mori, T., Kuroda, Y., Yoshikawa, Y., Nagao, M., Kittaka, S., 2002. Preparation of a water-resistant siliceous MCM-41 sample through improvement of crystallinity and its prominent adsorption features. *Langmuir 18*, 1595–1603.
- Cornac, M., Janin, A., Lavallee, J.C., 1984. Application of FTIR spectroscopy to the study of sulfidation of Mo catalysts supported on alumina or silica (4000–400  $\text{cm}^{-1}$  range). *Infrared Phys. 24*, 143–150.
- Qu, Z.P., Huang, W.X., Zhou, S.T., Zheng, H., Liu, X.M., Cheng, M.J., Bao, X.H., 2005. Enhancement of the catalytic performance of supported-metal catalysts by pretreatment of the support. *J. Catal. 234*, 33–36.
- Dubray, F., Dib, E., Medeiros-Costa, I., Aquino, C., Minoux, D., van Daele, S., Nesterenko, N., Gilson, J.-P., Mintova, S., 2022. The challenge of silanol species characterization in zeolites. *Inorg. Chem. Front. 9*, 1125–1133.
- Lin, O.H., Akil, H.M., Ishak, Z.A.M., 2009. Characterization and properties of activated nanosilica/polypropylene composites with coupling agents. *Polym. Compos. 30*, 1693–1700.
- Kang, S., Hong, S.I., Choe, C.R., Park, M., Rim, S., Kim, J., 2001. Preparation and characterization of epoxy composites filled with functionalized nanosilica particles obtained via sol-gel process. *Polymer 42*, 879–887.
- Scott, S.L., Basset, J.M., 1994. Coordination chemistry on surfaces: a new method to graft rhenium(VII) oxide on highly dehydroxylated oxides. *J. Am. Chem. Soc. 116*, 12069–12070.
- Bunker, B.C., Haaland, D.M., Michalske, T.A., Smith, W.L., 1989. Kinetics of dissociative chemisorption on strained edge-shared surface defects on dehydroxylated silica. *Surf. Sci. 222*, 95–118.
- Liu, C., Wijewardena, D.P., Sviripa, A., Sampath, A., Flaherty, D.W., Paolucci, C., 2022. Computational and experimental insights into reactive forms of oxygen species on dynamic Ag surfaces under ethylene epoxidation conditions. *J. Catal. 405*, 445–461.
- Chen, C.-T., Sviripa, A., Verma, S., Paolucci, C., Flaherty, D.W., 2025. Reactions of surface peroxides contribute to rates and selectivities for  $\text{C}_2\text{H}_4$  epoxidation on silver. *ACS Catal. 15*, 1387–1398.
- Pu, T., Setiawan, A., Foucher, A.C., Guo, M., Jehng, J.-M., Zhu, M., Ford, M.E., Stach, E. A., Rangarajan, S., Wachs, I.E., 2023. Revealing the nature of active oxygen species and reaction mechanism of ethylene epoxidation by supported Ag/ $\alpha$ -Al<sub>2</sub>O<sub>3</sub> catalysts. *ACS Catal. 14*, 406–417.
- Qu, Z.P., Cheng, M.J., Huang, W.X., Bao, X.H., 2005. Formation of subsurface oxygen species and its high activity toward CO oxidation over silver catalysts. *J. Catal. 229*, 446–458.
- Zhang, X.D., Dong, H., Wang, Y., Liu, N., Zuo, Y.H., Cui, L.F., 2016. Study of catalytic activity at the Ag/Al-SBA-15 catalysts for CO oxidation and selective CO oxidation. *Chem. Eng. J. 283*, 1097–1107.
- Nagy, A.J., Mestl, G., Herein, D., Weinberg, G., Kitzelmann, E., Schlägl, F., 1999. The correlation of subsurface oxygen diffusion with variations of silver morphology in the silver–oxygen system. *J. Catal. 182*, 417–429.
- Miller, J.H., Joshi, A., Li, X., Bhan, A., 2020. Catalytic degradation of ethylene oxide over Ag/ $\alpha$ -Al<sub>2</sub>O<sub>3</sub>. *J. Catal. 389*, 714–720.
- Dubois, L.H., Zegarski, B.R., 1993. The bonding of alkoxy silanes to dehydroxylated silica surfaces: a new adhesion mechanism. *Abstr. Pap. Am. Chem. Soc. 205*, 88-PHYS.
- Pu, T., Setiawan, A., Lis, B.M., Zhu, M., Ford, M.E., Rangarajan, S., Wachs, I.E., 2022. Nature and reactivity of oxygen species on/in silver catalysts during ethylene oxidation. *ACS Catal. 12*, 4375–4381.
- Xiong, H., Zhu, X., Lu, S., Zhou, C., Xu, W., Zhou, Z., 2021. Enhancement of plasma-catalytic oxidation of ethylene oxide (EO) over Fe–Mn catalysts in a dielectric barrier discharge reactor. *Sci. Total Environ. 788*, 147741.